INTERNATIONAL JOURNAL FOR NUMERICAL METHODS IN FLUIDS
Int. J. Numer. Meth. Fluids 2007; **53**:1297–1314
Published online in Wiley InterScience (www.interscience.wiley.com). DOI: 10.1002/fld.1449

On level set modelling of bi-fluid capillary flow

Anne-Cécile Lesage[1,2,*,†], Olivier Allain[1] and Alain Dervieux[1,2]

[1]*LEMMA, 938-A, avenue de la république, 06550 La Roquette-sur-Siagne, France*
[2]*INRIA, BP 93, 2004 route des Lucioles, 06902 Sophia-Antipolis, France*

SUMMARY

We consider the adaptation of a level set (LS) method for the simulation of capillary flows on unstructured meshes. The advection step is first analysed. In order not to lose accuracy, this step should be one order more accurate than the discretization of the velocity. We then compare different ways in choosing the LS velocity and in re-initializing the LS function between advection phases without losing too much accuracy. Applications to Rayleigh flows and to reorientation with contact angle are presented. Copyright © 2007 John Wiley & Sons, Ltd.

Received 14 December 2005; Revised 20 October 2006; Accepted 24 October 2006

KEY WORDS: incompressible Navier–Stokes; finite element method; interface tracking; capillarity; contact angle

1. INTRODUCTION

Interface motion simulation has been studied from the early start of computer simulation. The level set (LS) principle introduced in the late 1980s by Osher and Sethian [1–3] proposes to advect a relatively smooth field ϕ the zero contour of which is the interface to represent. Since the function to advect is smooth (in contrast to the usual step function), this method opens the door to an accuracy higher than first order.

The LS method extends to capillarity effects, see, for example, Sussman *et al.* [4, 5]. The idea of using volumic functions rather than surface tracking extends to surface tension modellization, by relying on function ϕ's volumic derivatives, according to ideas inspired by the work [6] of Brackbill *et al*. We shall review how the LS can be described as a purely differential model.

*Correspondence to: Anne-Cécile Lesage, LEMMA, 938-A, avenue de la république, 06550 La Roquette-sur-Siagne, France.
†E-mail: aclesage@gmail.com

Contract/grant sponsor: Région Provence-Alpes Côte d'Azur

As concerns discretization, LS has been most usually associated with Cartesian discretizations. Indeed the ancient, but still very attractive, Marker and Cell (MAC) approximation for incompressible flow can be applied to them. They also allow an easier development of high order accurate schemes. Most of all, in our opinion, Cartesian discretizations generally not only enjoy convergence of dependent variables but also enjoy convergence of their derivatives, and this can be paramount for surface tension modellization, which uses second derivatives of the solution of a (first-order) advection equation.

The LS method also combines well with a finite-element discretization, the intrinsic interpolation of which accurately specifies the interface location. Further, the combination of LS and finite element lends itself to discretization on unstructured meshes. However, when leaving the comfortable Cartesian case, we need to pay attention in order to obtain for the global scheme an order of accuracy better than unity for the interface advection. We propose an analysis which suggests to advect the LS function with higher precision with respect to the target accuracy for the interface motion. Further, in contrast to Cartesian meshes, surfaces traces and derivatives on unstructured meshes, may have poor convergence to continuous analog, if any. For example, computing second derivatives with linear Lagrangian finite elements deserves some attention. In [7, 8], Smolianski proposes to apply recent superconvergent schemes and this paper applies the same method. We evaluate our analysis on the calculation of a Rayleigh capillary instability.

Besides the numerical modelling of surface tension, a second important issue in capillarity flows is the numerical modelling of the contact angle. We found very few publications discussing numerical methods for this effect. In [9] where a Volume of Fluid (VOF) interface representation is used, the contact angle is built from a geometrical reconstruction of the interface. In this paper, we discuss the adequation of LS function and velocity extensions to contact angle modelling. We propose and compare two approaches.

The paper is organized as follows. The next section recalls the main features of LS method. In Section 3, by analysing the advection step, we give a lower estimate of the accuracy of the method under gradient conditions. Section 4 completes the numerical model description. Section 5 examines some means of extending the LS function without introducing new error sources. We propose a family of formulations which permits to accurately take into account the local orientation of a solid wall. Sections 6 and 7 are devoted to the experimentation of the proposed options for capillary flows with and without contact angle.

2. MAIN FEATURES OF THE LEVEL SET METHOD

Let us consider the following model for the flow of two incompressible immiscible fluids with interface tension

$$\rho\frac{\partial \mathbf{U}}{\partial t}+\rho\nabla\cdot(\mathbf{U}\otimes\mathbf{U})-\nabla\cdot(2\mu(\rho)\mathbf{D})+\nabla p+\sigma\kappa(\rho)\delta(\rho)\mathbf{n}-\rho\mathbf{g}=0$$

$$\partial_t\rho+\nabla\cdot(\rho\mathbf{U})=0,\quad \rho=\rho_{\mathrm{l}}\text{ or }\rho_{\mathrm{g}} \tag{1}$$

$$\nabla\cdot\mathbf{U}=0$$

In this formulation, the fluid velocity is denoted by $\mathbf{U}$, and the pressure by p. The density ρ takes only two values in two subdomains separated by an interface sufficiently smooth to compute the

DOI: 10.1002/fld

surface normal

$$\mathbf{n}\delta(\rho) = \frac{1}{\rho_\mathrm{l} - \rho_\mathrm{g}} \nabla \rho \tag{2}$$

further, $\delta(\rho)$ denotes the Dirac delta function on the interface, σ the surface tension coefficient, $\kappa(\rho)$ the curvature of the interface, $\mathbf{g}$ the gravity volumic force, $\mathbf{D} = \frac{1}{2}(\nabla \mathbf{U} + \nabla(\mathbf{U})^\mathrm{T})$ the deformation tensor, $\mu(\rho)$ the dynamic viscosity and ρ_l, ρ_g the two values taken by the density in each fluid. Typically, ρ_l in the liquid and ρ_g in the gas. In the case where $\sigma = 0$ and $\mu(\rho)$ is a constant, this model is a particular case of the heterogeneous Navier–Stokes model as analysed in [10]. The interface advection can be written with the characteristic function χ of liquid phase

$$\frac{\partial \chi}{\partial t} + \mathbf{U} \cdot \nabla \chi = 0 \quad (\chi = 0 \text{ or } 1), \quad \rho = \chi \rho_\mathrm{l} + (1 - \chi)\rho_\mathrm{g}$$

The formal accuracy of the advection of a step function as χ is severely limited to first order unless the numerical scheme exploits the fact that χ takes only two different values. A particular way of doing this is the second-order VOF method (see, for example, [11]) which we do not discuss further here. Let H be the step function such that $H(x) = 1$ if $x > 0$ and $H(x) = 0$ elsewhere. The LS method introduced by Osher and Sethian [1] relies on a smooth function ϕ satisfying $\chi = H(\phi)$

$$\frac{\partial \phi}{\partial t} + \mathbf{U} \cdot \nabla \phi = 0, \quad \chi = \mathrm{H}(\phi) \tag{3}$$

ϕ is initialized and periodically reset as the signed-distance to the interface $\phi = \pm d(\Gamma)$ [2, 3].

We take $\phi < 0$ in the gas region and $\phi > 0$ in the liquid region. The interface is the zero LS of ϕ.

$$\Gamma = \{\mathbf{x} | \phi(\mathbf{x}, t) = 0\} \tag{4}$$

Using the ϕ function, the previous governing equation for the fluid velocity $\mathbf{U}$ and the pressure p along with boundary conditions can be written as a single equation with a continuous surface force [6] formulation of the surface tension term [5],

$$\rho(\phi)\frac{\mathrm{D}\mathbf{U}}{\mathrm{D}t} = -\nabla p + \nabla \cdot (2\mu(\phi)\mathbf{D}) - \sigma\kappa(\phi)\delta(\phi)\nabla(\phi) + \rho(\phi)\mathbf{g}, \quad \nabla \cdot \mathbf{U} = 0 \tag{5}$$

The surface tension force is modelled as a volumic interfacial force on a thickened interface. $\kappa(\phi)$ is the curvature computed in all the domains as the second derivative of ϕ

$$\kappa(\phi) = \nabla \cdot (\mathbf{n}) = \nabla \cdot \left(\frac{\nabla \phi}{|\nabla \phi|} \right) \tag{6}$$

The density and the viscosity are constant in each fluid, we can write

$$\rho(\phi) = \rho_\mathrm{g} + (\rho_\mathrm{g} - \rho_\mathrm{l})H(\phi), \quad \mu(\phi) = \mu_\mathrm{g} + (\mu_\mathrm{g} - \mu_\mathrm{l})H(\phi)$$

The most usual LS method can be defined rather accurately according to the following stages:

Stage 1: define an advection velocity $\mathbf{V}$ for the LS.
Stage 2: advect the ϕ function with velocity $\mathbf{V}$ from time level n to time level $n + 1$.

DOI: 10.1002/fld

Stage 3: replace the advected $\bar{\phi}^{n+1}$ by a reinitialized or redistanced $\tilde{\phi}^{n+1}$ in order to satisfy at each time step the condition

$$\text{meas}(-\eta \leqslant \tilde{\phi}^{n+1} \leqslant \eta) \leqslant K_1 \eta \tag{7}$$

Stage 4: replace the re-initialized $\tilde{\phi}^{n+1}$ by a ϕ^{n+1} enjoying a conservation property.
Stage 5: compute with (6) a volumic extension $\kappa(\phi)$ of the zero contour curvature.
Stage 6: advance Equation (5) for moments.

The usual choice for $\mathbf{V}$ is $\mathbf{V} = \mathbf{U}$. Other options are discussed in Section 5. Stage 4 is needed only for the spatially discrete case and will be discussed in Section 4. The justification of Condition (7) is given in next section.

3. ERROR ANALYSIS OF LEVEL SET ADVECTION

This section is devoted to justifying Condition (7) and gives elements to choose the spatial discretization. Let us assume that we know how to numerically advect the LS ϕ by approximating it with a discrete LS function ϕ_h. Since ϕ is advected with a first-order hyperbolic model, according to variational theory, the usual convergence property for ϕ_h on non-regular meshes is a convergence in L^p, but we can manage a high order k of accuracy in that norm. Let us examine the consequence for the corresponding $\chi_\phi = H(\phi)$ functions.

Proposition 1
Let ϕ be a $L^p(Q)$ function where $Q = \Omega \times]0, T[$ is the flow integration domain in space and time. Let $(\phi_h)_h$ a sequence of $L^p(Q)$ we assume that

$$\text{meas}(-\eta \leqslant \phi \leqslant \eta) \leqslant K_1 \eta \tag{8}$$

$$\|\phi_h - \phi\|_{L^p(Q)} \leqslant K_2 h^k \tag{9}$$

with h, η sufficiently small, k the convergence order on ϕ and K_1, K_2 independent of h, η then for all real number $q \geqslant 1$, there is a constant $C(q)$ independent of h such as

$$\|H(\phi_h) - H(\phi)\|_{L^q(Q)} \leqslant C(q) h^{2k/3q} \tag{10}$$

Proof
the above integral can be analysed as follows:

$$\begin{aligned}\int_Q |H(\phi_h) - H(\phi)| \, \mathrm{d}\Omega \, \mathrm{d}t &\leqslant \text{meas}(|\phi| \leqslant \eta) + \text{meas}(|\phi_h| \leqslant \eta) \\ &\quad + \text{meas}(\phi \geqslant \eta, \phi_h \leqslant -\eta) + \text{meas}(\phi \leqslant -\eta, \phi_h \geqslant \eta) \\ &\leqslant \text{meas}(|\phi| \leqslant \eta) + \text{meas}(|\phi_h| \leqslant \eta) + \text{meas}(|\phi_h - \phi| \geqslant 2\eta)\end{aligned}$$

but

$$\text{meas}(|\phi| \leqslant \eta) \leqslant K_1 \eta \quad \text{according to (8)}$$

DOI: 10.1002/fld

and

$$\text{meas}(|\phi_h|\leqslant\eta)\leqslant\text{meas}(|\phi|\leqslant 2\eta)+\text{meas}(|\phi_h-\phi|\geqslant\eta)$$

that is

$$\text{meas}(|\phi_h|\leqslant\eta)\leqslant 2K_1\eta+\text{meas}(|\phi_h-\phi|\geqslant\eta)$$

thus

$$\int_Q |H(\phi_h)-H(\phi)|\,\mathrm{d}\Omega\,\mathrm{d}t\leqslant 3K_1\eta+2\,\text{meas}(|\phi_h-\phi|\geqslant\eta) \tag{11}$$

The last sum part can be estimated as follows:

$$\text{meas}(|\phi_h-\phi|\geqslant\eta)=\int_{|\phi_h-\phi|^p\geqslant\eta^p} 1\,\mathrm{d}\Omega\,\mathrm{d}t\leqslant\frac{1}{\eta^p}\int_{|\phi_h-\phi|^p\geqslant\eta^p}|\phi_h-\phi|^p\,\mathrm{d}\Omega\,\mathrm{d}t\leqslant\frac{1}{\eta^p}\|\phi_h-\phi\|^p_{L^p(Q)} \tag{12}$$

and with (11) and (12), we get

$$\int_Q |H(\phi_h)-H(\phi)|\,\mathrm{d}\Omega\,\mathrm{d}t\leqslant 3K_1\eta+\frac{2}{\eta^p}\|\phi_h-\phi\|^p_{L^p(Q)}$$

By choosing $\eta=h^\theta$, $\theta=pk/(p+1)$, we get

$$\int_Q |H(\phi_h)-H(\phi)|\,\mathrm{d}\Omega\,\mathrm{d}t\leqslant 3K_1h^\theta+2K_2^2h^{-p\theta}h^{pk}\leqslant(3K_1+2K_2^2)h^{pk/(p+1)}$$

thus

$$\int_Q |H(\phi_h)-H(\phi)|\,\mathrm{d}\Omega\,\mathrm{d}t\leqslant(3K_1+2K_2^2)h^{pk/(p+1)}$$

or equivalently, for $q\geqslant 1$

$$\|H(\phi_h)-H(\phi)\|_{L^q}\leqslant K_5h^{pk/q(p+1)} \tag{13}$$

□

Remark 1
Estimate (13) is not optimal and the order of accuracy is located between $pk/q(p+1)$ and k. However, the possible loss of accuracy shown in (13) is related to inaccuracy on the interface when ϕ_h is not sufficiently smooth. In practice, ϕ_h can be re-initialized, but this may introduce other errors. In the sequel, we shall refer to the case $p=2, q=1$, which gives an order between $2k/3$ and k.

The above analysis suggests that, in order to get a global second-order convergence for a LS multifluid calculation, a second-order Navier–Stokes approximation should be combined with a *third-order* accurate advection of the function ϕ. This is the option taken in the rest of the paper.

DOI: 10.1002/fld

4. SPATIAL DISCRETIZATION

In the computations presented, the six-stage LS algorithm of Section 2 is spatially discretized on a 2D triangulation by considering all main variables in the usual finite element V_h space of continuous, elementwise linear functions, with degrees of freedom at triangle vertices

$$\mathbf{U} \in (V_h)^2, \quad p \in V_h, \quad \phi \in V_h, \quad \kappa \in V_h \tag{14}$$

Most discretization options of [7] are adopted (in particular a projection algorithm for moments). We deviate from this rule for the advection of ϕ by advecting it with an upwind biased scheme of second-order accuracy on general meshes and third-order accuracy on Cartesian meshes (see [12]). As redistancing is concerned, several authors recommend to build a signed distance by iterating until steady-state a Hamilton–Jacobi equation (see [2, 3, 5]). In our study, we follow Smolianski [7] and our basic option is to rebuild a distance from a geometrical algorithm, defining ϕ_{dist} at each vertex as the minimum distance to discrete zero level of ϕ. In stage 4, we use a global volume conservation correction slightly different from that of [7]; a small perturbation C_ϕ is added to ϕ in each point of the domain in order to solve iteratively the following conservation relation:

$$\overline{\phi}_h^{n+1} = \phi_h^{n+1} + C_{\phi_h}, \quad \int H(\overline{\phi}_h^{n+1})\,\mathrm{d}v = \int H(\phi_h^n)\,\mathrm{d}v$$

5. INTERFACE VARIABLES EXTENSION

The LS method relies on the representation of several variables defined on the interface as volumic variables:

- the interface location is extended into a LS function;
- the interface velocity is used under a volumic shape;
- for capillarity, the interface normal and curvature also become volumic fields.

We observe that there are some constraints on these representations. They must be sufficiently smooth, easy to compute accurately. Lastly, Condition (7) on LS gradient is a rather constraining one. However, these conditions still allow for many possible choices between the possible extensions of the above variables. The purpose of the reinitialization Stage 3 is to replace function ϕ by a new one of same zero contour but satisfying Condition (7). Further, this new function should be sufficiently smooth to permit an accurate computation of interface curvature. In the discrete case, there is no guarantee that the new function has exactly the same zero contour, nor that it will be sufficiently smooth. If the advection step provides a ϕ function which already satisfies the unit gradient condition, at least close to interface, we can imagine that the error in the reinitialization step can be made smaller, because the reinitialization step does not need large changes of function ϕ or even does not need changing it at all. However, we need to check whether the global algorithm has an increased accuracy. In order to study these points, we propose to *reconsider either interface motion direction*, *or the extension of LS function from interface*, which concerns Stage 3 (both option can also be combined).

DOI: 10.1002/fld

5.1. Level set extensions

LS function's gradient has to be controlled in order to satisfy condition (7). In usual LS method, this is performed by two means: (a) a canonical extension of the zero level is built with a signed distance, and (b) LS function is advected with the material velocity $\mathbf{U}$. To build a more general context, we identify two design criteria:

- control of LS gradient;
- consistent interface motion;

and we consider two main choices:

- the canonic LS extension;
- the interface velocity.

We restrict to 2D case for simplicity.

5.1.1. Consistent interface motion. Let us return to the advection of the characteristic function χ which writes (in sense of distributions)

$$\frac{\partial \chi}{\partial t} + \mathbf{U} \cdot \nabla \chi = 0 \quad (\chi = 0 \text{ or } 1) \tag{15}$$

Let $\mathbf{n}_\chi$ be the normal vector to the interface Γ and $\boldsymbol{\tau}_\chi$ the tangential vector to the interface, i.e. such as $\nabla \chi \cdot \boldsymbol{\tau}_\chi = 0$. The function χ is equivalently advected with any velocity $\mathbf{V}'$ such that

$$(\mathbf{U} - \mathbf{V}') \cdot \mathbf{n}_\chi = 0 \quad \text{on } \Gamma \ \ \forall t > 0 \tag{16}$$

To parameterize the set of possible $\mathbf{V}'$ over the whole computational domain we first introduce a unit field specifying in the whole domain the direction of motion. Let $\widetilde{\mathbf{V}}_\Gamma$ be a vector defined on Ω such that

$$\widetilde{\mathbf{V}}_\Gamma \cdot \mathbf{n}_\chi \neq 0$$

$$|\widetilde{\mathbf{V}}_\Gamma| = 1$$

If we construct a scalar field α such that

$$\alpha = \frac{\langle \mathbf{V}, \mathbf{n}_\chi \rangle}{\langle \widetilde{\mathbf{V}}_\Gamma, \mathbf{n}_\chi \rangle} \quad \text{on the interface}$$

then the vector field $\mathbf{V}' = \alpha \widetilde{\mathbf{V}}_\Gamma$ advects χ in an equivalent way to $\mathbf{U}$. To complete the definition of $\mathbf{V}'$, it remains to define an extension of α.

5.1.2. LS gradient control. We look for an advection step which conserves the streamline derivative of LS function in the neighbourhood of interface, i.e. which conserves the derivative of ϕ parallel to interface velocity. The interface velocity gradient should be zero in this neighbourhood. We need a streamline constant extension operator for this velocity.

DOI: 10.1002/fld

Constant extension: $\alpha \mapsto \widetilde{S}\alpha$: given α on the interface, we can extend it along the field $\widetilde{\mathbf{V}}_\Gamma$ by imposing its extension $\widetilde{S}\alpha$ to be constant on each trajectory. This extends the interface velocity $\mathbf{V}'$

$$\widetilde{\mathbf{V}}_\Gamma \cdot \nabla \widetilde{S}\alpha = 0 \tag{17}$$

$$\mathbf{V}' = \widetilde{S}\alpha \widetilde{\mathbf{V}}_\Gamma \tag{18}$$

In a dual manner, the corresponding extension operator for ϕ is a constant-gradient extension operator

Constant-gradient extension: $\phi \mapsto \widetilde{P}\phi$: given a scalar field ϕ on the interface, we can define $\widetilde{P}\phi$ as the function equal to ϕ on the interface and such that

$$\widetilde{\mathbf{V}}_\Gamma \cdot \nabla \widetilde{P}\phi = 1 \tag{19}$$

The main properties of our construction is now summed up.

Proposition 2
Starting from a LS function satisfying the gradient property (19), for example defined as $\widetilde{P}\phi$, and advecting it with the streamline constant extension $\mathbf{V}' = \widetilde{S}\alpha \widetilde{\mathbf{V}}_\Gamma$

$$\frac{\partial \widetilde{P}\phi}{\partial t} + \widetilde{S}\alpha \widetilde{\mathbf{V}}_\Gamma \cdot \nabla \widetilde{P}\phi = 0 \tag{20}$$

will produce an advected ϕ which still satisfies the gradient property (19) in the vicinity of interface.

Proof
We assume that we can construct a prolongation of ϕ such that

$$\nabla \widetilde{P}\phi \cdot \widetilde{\mathbf{V}}_\Gamma = 1 \quad \text{with } \widetilde{\mathbf{V}}_\Gamma \text{ constant in time}$$

To demonstrate that $\nabla \widetilde{P}\phi \cdot \widetilde{\mathbf{V}}_\Gamma$ is constant in time, we use (17), (19) and (20)

$$\frac{\delta(\nabla \widetilde{P}\phi \cdot \widetilde{\mathbf{V}}_\Gamma)}{\delta t} = \frac{\nabla \widetilde{P}\phi}{\delta t} \cdot \widetilde{\mathbf{V}}_\Gamma = \nabla \left(\frac{\widetilde{P}\phi}{\delta t} \right) \cdot \widetilde{\mathbf{V}}_\Gamma = -\nabla(\widetilde{S}\alpha \widetilde{\mathbf{V}} \cdot \nabla \widetilde{P}\phi) \cdot \widetilde{\mathbf{V}}_\Gamma = -\nabla \widetilde{S}\alpha \cdot \widetilde{\mathbf{V}}_\Gamma = 0 \qquad \square$$

5.2. A dilemma

The important consequence of Proposition 2 is that since (19) is satisfied, the reinitialization will not introduce a large error or can in some case be purely skipped. However, the operation of taking the trace of the velocity $\mathbf{U}$ on the interface Γ introduces a new error which needs to be analysed. Let us analyse the system as if it were an elliptic second-order one. The functional space to do this is the Sobolev space H^s of functions with square integrable derivative up to order s. This definition extends to fractional s through local Fourier transforms. We assume that

- either the velocity is a smooth known function $\mathbf{U}$ which we interpolate on P_1 functions. $\mathbf{U}_h = \Pi_h \mathbf{U}$. then for $s = 0$ and 1

$$\|\mathbf{U}_h - \mathbf{U}\|_{H^s} = \|\Pi_h \mathbf{U} - \mathbf{U}\|_{H^s} \leqslant K_1(\mathbf{U}) h^{2-s} \tag{21}$$

DOI: 10.1002/fld

- or the velocity is accurately computed from a discretized system satisfying the following error estimate:

$$\|\mathbf{U}_h - \mathbf{U}\|_{H^s} \leqslant K_2(\mathbf{U}) h^{2-s} \tag{22}$$

By the trace theorem and by the convexity inequality, we get

$$\|\mathbf{U} - \mathbf{U}_h\|_{L^2(\Gamma)} \leqslant K_3(\mathbf{U}) \|\mathbf{U} - \mathbf{U}_h\|_{H^{1/2}} \leqslant K_4(\mathbf{U}) \|\mathbf{U} - \mathbf{U}_h\|_{H^0}^{1/2} \|\mathbf{U} - \mathbf{U}_h\|_{H^1}^{1/2} \leqslant K_5(\mathbf{U}) h^{3/2} \tag{23}$$

where K_1, K_2, K_3, K_4, K_5 depend on $\mathbf{U}$ but not of h. This means that working with any extension of the velocity from its trace on the interface implies a loss of accuracy order with a gap of $\frac{1}{2}$, in particular.

Proposition 3
With a second-order accurate Navier–Stokes scheme, a global accuracy of $\frac{3}{2}$ holds.

To sum it up, it is possible to build a velocity field which to some degree avoids the error associated with redistancing, but some other loss of accuracy may arise, especially when irregular/unstructured meshes are used, due to the fact that we take a trace of advection velocity on the interface.

5.3. Provisional conclusion

We have identified a general class of interface velocity and extension. The impact on global accuracy is analysed. In the absence of wall effect, reinitialization by a signed distance can be improved by increasing the consistency of the combined advection and redistancing steps. When the problem under study involves a contact angle condition, we shall choose in Section 7 a different reinitialization.

6. FIRST EXPERIMENT: CAPILLARY INSTABILITY

This section is devoted to illustrate Section 3. We investigate how accurate is the LS algorithm based on a reinitialization by signed distance and the third-order advection scheme of the LS function. We consider the Rayleigh instability of a liquid cylinder in the case where capillary effects are dominant. The cylinder is perturbed with a perturbation equation in the half plane ($x>0$) containing the symmetry axis of the cylinder defined as

$$x = a + \eta \sin\left(\frac{2\pi y}{\lambda_d} + K_1\right) \tag{24}$$

in which λ_d and η are, respectively, the wave length and the perturbation height. For $\lambda_d > 2\pi a$ where a is the liquid cylinder radius, the perturbation amplifies (Figure 1).

We use the numerical algorithm, stage 1 to stage 6, described in the second section, with:

- an axisymmetric formulation;
- a geometric redistancing of ϕ every 10 time steps;
- a mass conservation of each disconnected liquid phase in the manner described at the end of Section 4.

DOI: 10.1002/fld

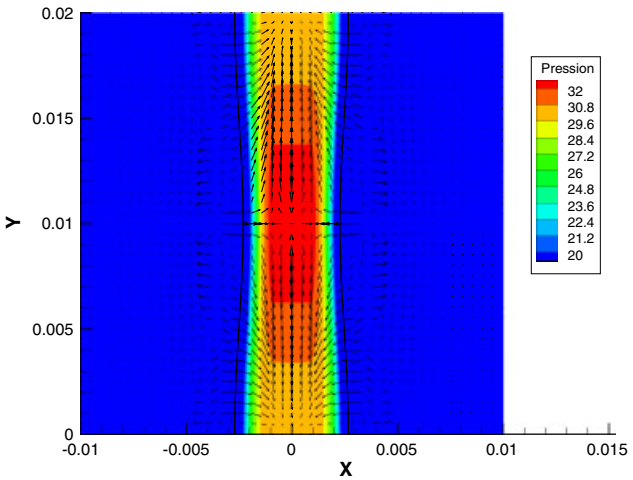

Figure 1. Initialization of the perturbation. Visualization of pressure field, velocity vectors and interface (black line).

Table I. Test case: capillary instability.

Surface tension coefficient	$\sigma = 0.07275$ SI
Liquid cylinder radius	$r = 0.01$ m
Density ratio	$\rho_l = 1000\,\mathrm{kg\,m^3}$, $\rho_g = 1.2\,\mathrm{kg\,m^3}$
Computation domain size	$L_x = 0.01$ m, $L_y = 0.02$ m
$a = 0.0025$ m, $\lambda_d = 0.02$ m	

According to the previous analysis, a global spatial accuracy of second order should hold for regular cases.

We measure the numerical order of accuracy before and after the formation of a drop. The different parameters of the test case are described in Table I. We compare the results obtained with three meshes embedded with, respectively, 902, 3402 and 13 202 mesh nodes (grid space step, respectively, of $4h$, $2h$ and h with $h = 0.125$ mm). Time discretization error is kept small by *ad hoc* choices of time steps.

The breaking occurs at $t = 0.136$ s for the coarse mesh, $t = 0.125$ s for the intermediate mesh and $t = 0.122$ s for the fine mesh. We measure the convergence of both the L_2 error norm of ϕ and the L_1 error norm of $H(\phi)$ at $t = 0.11$ s (before the breaking for the three meshes) $t = 0.12$ and 0.13 s (after the breaking for all meshes). Figures 2 and 3 representing the mesh convergence on interface location at $t = 0.11$, 0.12 and 0.13 s give already a visual idea of the loss of accuracy. Table II shows the convergence order on the deviations $\|\phi_h - \phi_{2h}\|_{L_2}$, where ϕ's are redistanced, and $\|H(\phi_h) - H(\phi_{2h})\|_{L_1}$ between embedded meshes. The numerical convergence order is evaluated through computations on three embedded meshes by the following equation:

$$n = \frac{\log\left(\dfrac{\|\Psi_{2h} - \Psi_{4h}\|}{\|\Psi_h - \Psi_{2h}\|}\right)}{\log(2)} \tag{25}$$

DOI: 10.1002/fld

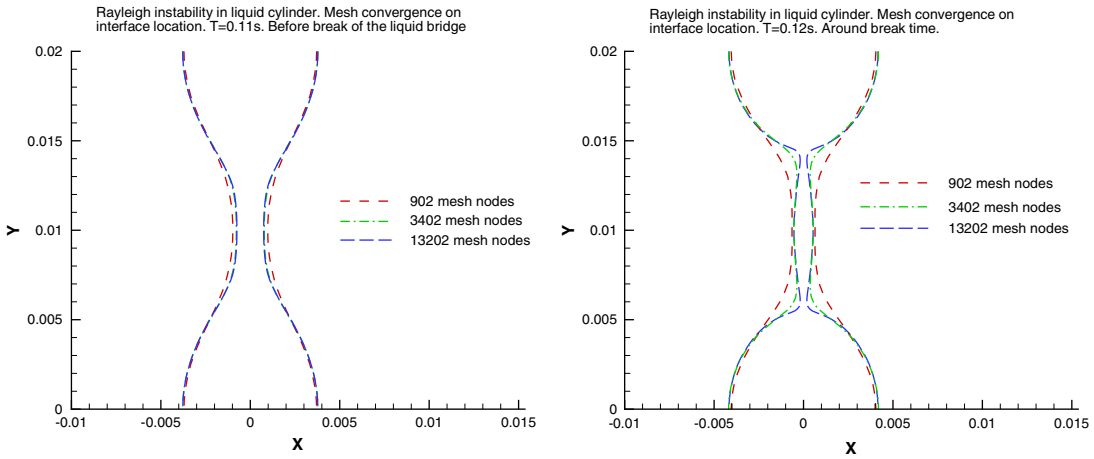

Figure 2. Left: mesh convergence on interface at $T = 0.11$ s. Right: mesh convergence on interface at $T = 0.12$ s.

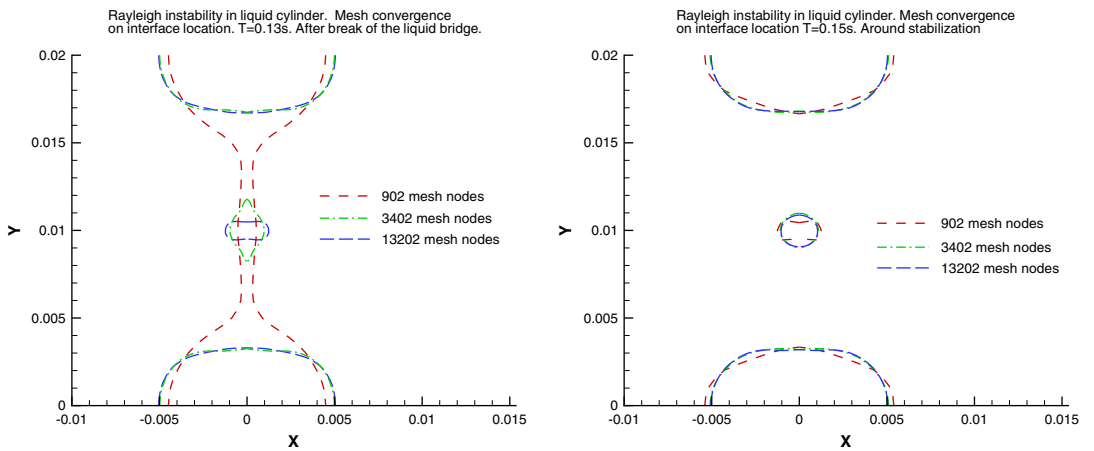

Figure 3. Left: mesh convergence on interface at $T = 0.13$ s. Right: mesh convergence on interface at $T = 0.15$ s (medium and fine outputs are very close to each other).

where Ψ_h, Ψ_{2h} and Ψ_{4h} are discrete solutions on the mesh with h, $2h$ and $4h$ as space step.

Results for time $t = 0.11$ illustrate the case for which our error analysis of Section 3 should apply. Redistanced ϕ's converge with an order smaller than 3. Conversely, for these very smooth interfaces, interfaces converge uniformly and with a numerical order of three, i.e. more than expected from the accuracy of the global Navier–Stokes scheme. Time $t = 0.12$ results still show approximately second-order numerical order. At time $t = 0.13$, breaking has occurred for medium and fine meshes but not yet for the coarse-mesh computation. The accuracy on that coarse mesh is

DOI: 10.1002/fld

Table II. Capillary instability.

Physical time (s)	Grid size	L_2 deviation on ϕ	L_1 deviation on $H(\phi)$
0.11	902	—	—
0.11	3402	1.6253×10^{-6}	2.45461×10^{-6}
0.11	13 202	2.46967×10^{-7}	3.23397×10^{-7}
0.11	Numerical order	2.7	2.92
0.12	902	—	—
0.12	3402	2.982×10^{-6}	5.515×10^{-6}
0.12	13 202	7.915×10^{-7}	1.520×10^{-6}
0.12	Numerical order	1.91	1.86
0.13	902	—	—
0.13	3402	9.33789×10^{-6}	1.38947×10^{-5}
0.13	13 202	3.233×10^{-6}	2.236×10^{-6}
0.13	Numerical order	1.53	2.63

Note: Numerical order on the interface position at $t = 0.11$, 0.12, and 0.13 s.

much degraded for the ϕ function. The level of error for $H(\phi)$ becomes also high for the coarse mesh and the high numerical order measured is not significative of anything but the large error of coarse mesh.

7. APPLICATION TO CAPILLARITY WITH CONTACT ANGLE

We consider now the numerical modelling of axisymmetric capillary effects with gravity and contact angle in a vertical tube. In the differential model that we study, a prescribed static angle β_S is satisfied by the interface. In terms of the LS function, this means that at contact point A we have

$$\nabla\phi(A) \cdot \mathbf{n}_\Sigma = \cos(\beta_S) \tag{26}$$

Since β_S is generally not equal to $\pi/2$, the corresponding signed distance to interface is not smooth in the vicinity of the contact point. A consequence is that the interface curvature is more difficult to evaluate from the LS function (6) as we can observe in Figure 4. We need to consider another option for reinitialisation of ϕ. In this section, we propose an axial velocity field construction and an axial extension operator and we study their impact on the computation of the reorientation of a free surface after a sudden decreasing of gravity to zero.

7.1. Axial velocity field and axial extension operator

With the particular geometry of a tube, we can use a very simple particular case of the previous theory. We take as velocity $\widetilde{\mathbf{V}}_\Gamma$ the constant unitary field parallel to vertical axis

$$\widetilde{\mathbf{V}}_\Gamma = e_z$$

At an instant t, we extend the LS function from the interface position ($\phi_\Gamma = 0$) along e_z, with

$$\frac{\delta\phi}{\delta z} = 1 \tag{27}$$

DOI: 10.1002/fld

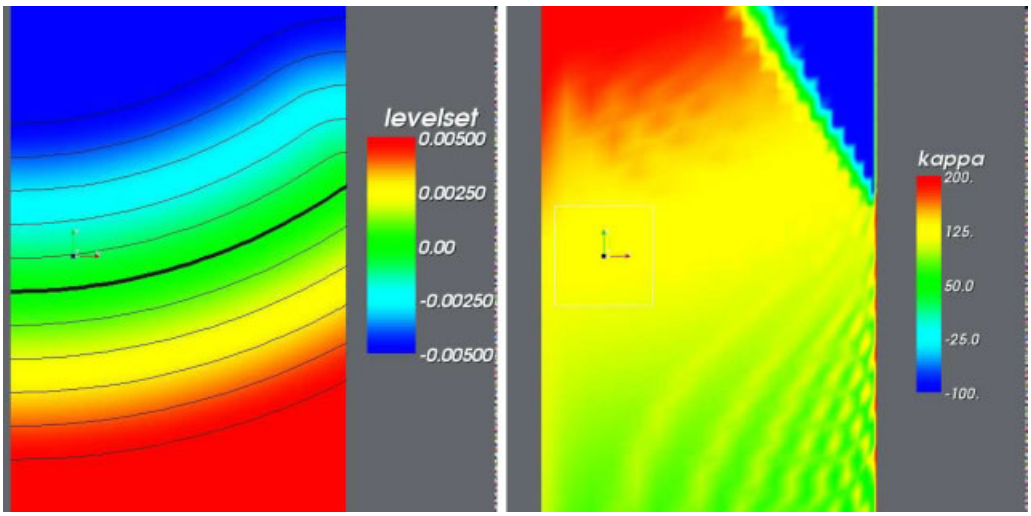

Figure 4. Equilibrium circular meniscus with contact angle. Left: signed distance ϕ function. The thickened line represents the interface. Right: curvature 'κ' computed as 2nd derivative of ϕ.

Let $h_p = f(r)$ be the bijection representing the interface. We define function ϕ's z-affine extension with

$$\phi(r, z) = -(z - h_p(r)) \tag{28}$$

As the representation of the interface can be represented as a bijection $h_p = f(r)$ and since the contact angle is not equal to zero for any point $M(r, z)$ of Γ, we have

$$e_z \cdot \mathbf{n}_\chi \neq 0$$

Then, according to the previous theory, we can derive a new velocity field $\mathbf{V}'$ as follows

$$\mathbf{V}' = \alpha e_z \quad \text{and} \quad \mathbf{V}' = (\mathbf{U} \cdot \mathbf{n}_\chi) \cdot \mathbf{n}_\chi + \beta \boldsymbol{\tau}_\chi$$

This choice allows the satisfaction of Condition (7) specified in Section 2 as far as the interface orientation does not show vertical parts, i.e. its normal is never orthogonal to z-axis.

$$\mathbf{V}'_r = 0 = ((\mathbf{U} \cdot n) \cdot n)_r + \beta \boldsymbol{\tau}_r \tag{29}$$

$$\mathbf{V}'_z = ((\mathbf{U} \cdot n) \cdot n)_z + \beta \boldsymbol{\tau}_z \tag{30}$$

$$\beta = \frac{-((\mathbf{U} \cdot n) \cdot n)_r}{\boldsymbol{\tau}_r} \tag{31}$$

$$\mathbf{V}'_z = \alpha e_z \quad \text{with } \alpha = ((\mathbf{U} \cdot n) \cdot n) \cdot e_z + \beta \boldsymbol{\tau}_z \tag{32}$$

In the whole domain $\mathbf{V}'(r, z) = \alpha(r) e_z$ where $\alpha(r)$ is the value of α at radius r on Γ. Figure 5 shows the desired transformation. The advancing of ϕ in time with $\mathbf{V}'(r, z)$ keeps the property $\phi(r, z) = -(z - h_p(r))$. On Figure 6, we can also observe how the extension of the ϕ function along e_z improves the computation of the curvature on a circular equilibrium interface compared to the case of ϕ as a signed distance to the interface.

DOI: 10.1002/fld

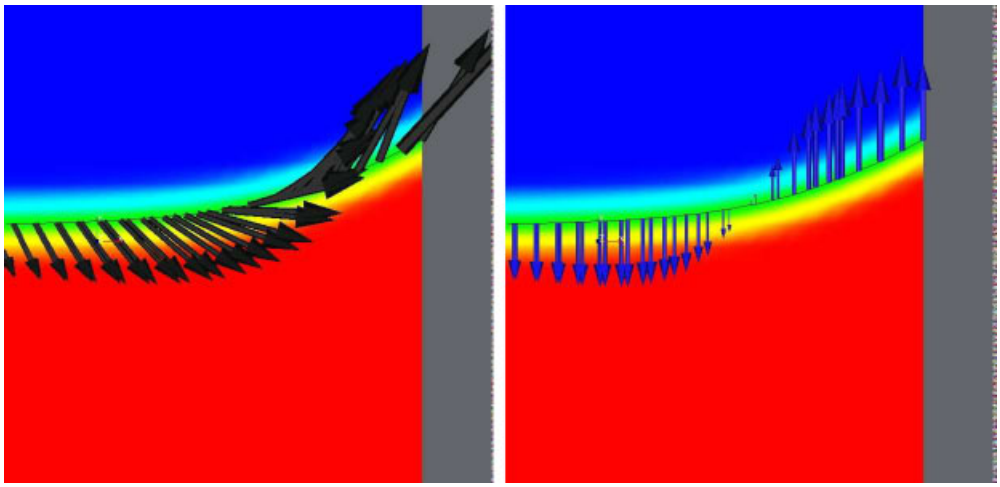

Figure 5. Transformation of the velocity field $\mathbf{U} \rightarrow \mathbf{V}' = \alpha\widetilde{\mathbf{V}}$ with $\widetilde{\mathbf{V}} = e_z$.

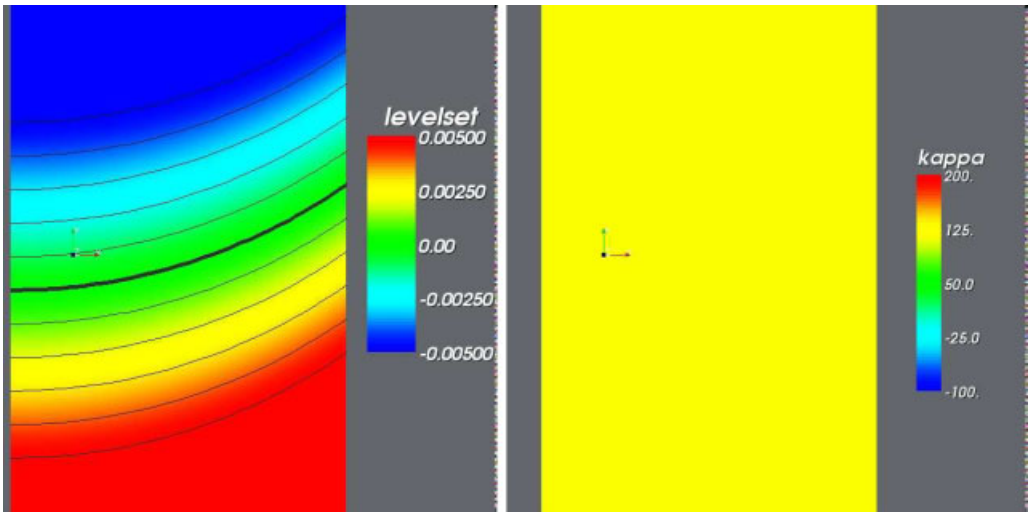

Figure 6. Equilibrium circular meniscus with contact angle. Left: ϕ function extended along e_z. Right: curvature 'κ' computed as 2nd derivative of ϕ extended along e_z. Thickened line represents the interface.

7.2. *Numerical results*

We consider the reorientation computation of a free surface in an axisymmetric vertical cylinder after a sudden decreasing of the gravity to zero. The motion is dominated by two effects, the surface tension force and the contact angle at wall. In this study, we are interested in numerical accuracy and we restrict our study to a constant contact angle model. This means that Condition

DOI: 10.1002/fld

Table III. Physical properties of liquid phase.

Dynamic viscosity of the liquid	2.566×10^{-3} kg m^{-1} s
Contact angle, θ_S	55°
Surface tension coefficient	$\sigma = 0.0181074$ SI
Cylinder radius	$r = 0.01$ m
Cylinder height	$h = 0.048$ m
Density values	$\rho_l = 879$ kg m^3, $\rho_g = 1.2$ kg m^3

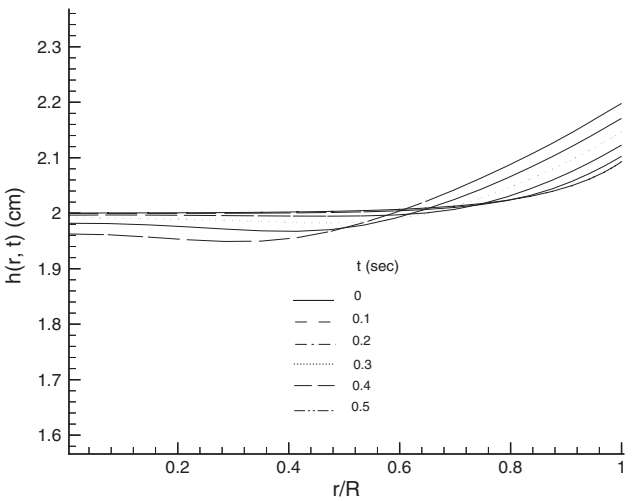

Figure 7. Capillary reorientation. Free surface evolution $t = 0.; 0.01; 0.02; 0.03; 0.04; 0.05$ s.

(26) is imposed at each time step. The liquid is M_3 with physical properties given in Table III. The gas is air. We refer to the works of ZARM research centre of Bremen, [9, 13, 14] for further details and for investigations of physical aspects of the problem under study.

Initial condition of the simulation is the equilibrium of a liquid in a cylindrical horizontal vessel under gravity and capillary forces. The gravity is suddenly shifted to zero. The liquid moves towards a new zero-gravity equilibrium, limited by a perfect spherical interface. We compute the reorientation transients over $t = 4.7$ s on four meshes embedded but not uniform (refined on the wall) with, respectively, 11, 21, 41, 81 grid nodes in the cylinder radius. Then third order accuracy of LS advection does not apply and accuracy can be limited to $\frac{4}{3}$ for the interface (Section 3), to be compared to the possible $\frac{3}{2}$ (or worse) limitation for an option using a trace of the velocity (Section 4). The initial equilibrium shows an interface which is essentially horizontal, flat at central region, with large curvature and contact angle at the wall. Figure 7 shows the smooth advection of the interface other the first 0.05 s. The interface position at wall rises monotonically. Figure 8 demonstrates that this rising continues after 0.1 s. Then the motion oscillates in a damped mode, converging to the new equilibrium. We propose a mesh convergence study for ϕ and $H(\phi)$ at time levels $t = 0.005, 0.01, 0.02$ s for two different schemes introduced below, in order to get a confirmation of the two estimates (13) and (23). The LS function ϕ is initialized

DOI: 10.1002/fld

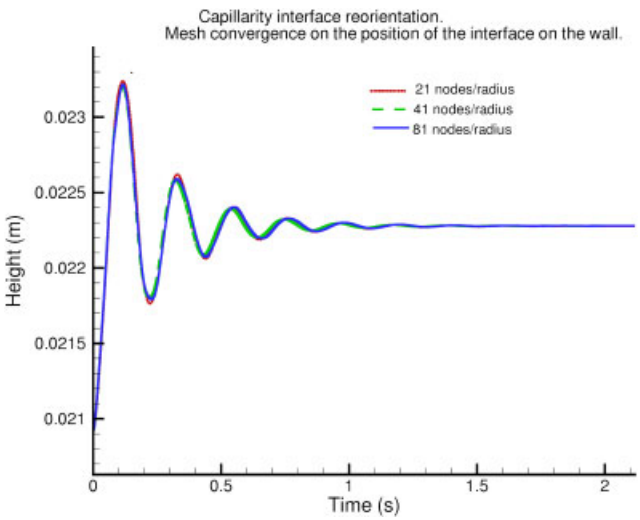

Figure 8. Capillary reorientation. Mesh convergence for the interface position on the wall.

Table IV. Capillary meniscus reorientation.

Number of nodes in the cylinder radius	L_2 deviation norm on ϕ	L_1 deviation norm on $H(\phi)$
11	—	—
21	1.06668×10^{-7}	3.40992×10^{-8}
41	5.32013×10^{-8}	1.45119×10^{-8}
Numerical order	1.003	1.233
81	2.51436×10^{-8}	4.73495×10^{-9}
Numerical order	1.081	1.62

Note: Numerical order on the deviation norms at $t = 0.005$ s for *Scheme* 1.

as the z-affine extension introduced in (28). Then we apply the two following advection schemes for ϕ:

Scheme 1: We advect ϕ with the axial velocity field (32) deduced from the physical velocity and apply no reinitialization.

Scheme 2: We advect ϕ with the physical velocity and we reinitialize the ϕ as the z-affine extension introduced in (28).

Figure 8 shows the mesh convergence on the time evolution of the interface position on the wall using *Scheme 2* for the computation. We measured a global second-order convergence on the contact point of interface location at the maxima of this curve ($t \approx 0.12$ s). To measure the convergence on global interface position, we consider the same norms as before, i.e. $\|\phi_h - \phi_{2h}\|_{L_2}$ and $\|H(\phi_h) - H(\phi_{2h})\|_{L_1}$. Tables IV and V show numerical convergence figures. Convergences of the deviation norm L_2 on ϕ are particularly poor, and less good for *Scheme 1* than for *Scheme 2*. The influence of redistancing (*Scheme 2*) may be rather large. For the *Scheme 1* result, the error in velocity trace can qualitatively explain, according to (23) the disappointing convergence. However,

DOI: 10.1002/fld

Table V. Capillary meniscus reorientation.

Number of nodes in the cylinder radius	L_2 deviation norm on ϕ	L_1 deviation norm on $H(\phi)$
11	—	—
21	1.10242×10^{-7}	3.43735×10^{-8}
41	4.72528×10^{-8}	1.38395×10^{-8}
Numerical order	1.22	1.31
81	1.84879×10^{-8}	4.70746×10^{-9}
Numerical order	1.35	1.555

Note: Numerical order on the deviation norms at $t = 0.005$ s for *Scheme* 2.

both schemes give about the same accuracy for the interface, an accuracy not so different from the $\frac{3}{2}$ and $\frac{4}{3}$ theoretical predictions.

8. CONCLUDING REMARKS

The LS principle introduces a smooth function ϕ in place of a step function, opening the door to higher-order accurate advection. We first analyse with only very few assumptions how higher order can be obtained, and under which conditions. We then define a larger set of possible LS re-initializations and of possible interface velocities constructions and we study the interaction between these options.

The first part of the analysis is confronted with the practical calculation of a capillary Rayleigh instability. In this flow, although a singularity appears at breaking time, the overall accuracy remains close to second order.

In the case of a capillarity phenomenon with contact angle, we propose to replace the signed distance by a generalized one in order to provide an accurate curvature field at contact point vicinity. Two options are compared. Either LS is solely extended or the interface velocity is also extended from the trace on interface. These options appear of equivalent accuracy and stability on the calculation of a zero-gravity interface re-orientation. In a general geometry, an extension of the proposed method would involve the evaluation of the parameterizing field by a numerical algorithm. Under this condition, the method would extend to 3D geometries.

ACKNOWLEDGEMENT

The first author was partly supported by a scientific scholarship of Région Provence-Alpes Côte d'Azur.

REFERENCES

1. Osher S, Sethian JA. Front propagating with curvature dependant speed: algorithms based on Hamilton–Jacobi formulations. *Journal of Computational Physics* 1988; **79**(12).
2. Sethian JA. *Level Set Methods and Fast Marching Methods*. Cambridge University Press: Cambridge, 1999.
3. Osher S, Fedkiw R. *Level Set Methods and Dynamic Implicit Surfaces*. Springer: Berlin, 2002.
4. Sussman M, Smereka P, Osher S. A level set approach for computing solutions to incompressible two-phase flow. *Journal of Computational Physics* 1994; **114**:146–159.
5. Sussman M, Fatemi E, Smereka P, Osher S. An improved level set method for incompressible two-phase flows. *Computers and Fluids* 1998; **27**(5–6):663–680.

DOI: 10.1002/fld

6. Brackbill J, Kothe DB, Zemach C. A continuum method for modeling surface tension. *Journal of Computational Physics* 1992; **100**:335–354.
7. Smolianski A. Finite-element/level-set/operator-splitting (FELSOS) approach for computing two-fluid unsteady flows with free moving interfaces. *International Journal for Numerical Methods in Fluids* 2005; **48**:231–269.
8. Smolianski A. Numerical modeling of two-fluid interfacial flows. *Ph.D. Thesis*, University of Jyvaskyla, Finland, 2001.
9. van Mourik S. Numerical modelling of the dynamic contact angle. *Master's Thesis*, Department of Mathematics, University of Groeningen, 2002.
10. Simon J. Non-homogeneous viscous incompressible fluids: existence of velocity, density and pressure. *SIAM Journal on Mathematical Analysis* 1990; **21**(5).
11. Pilliod Jr JE, Puckett EG. Second-order accurate volume-of-fluid algorithms for tracking material interfaces. *Journal of Computational Physics* 2004; **199**(2):465–502.
12. Gourvitch N, Rogé G, Abalakin I, Dervieux A, Kozubskaya T. A tetrahedral-based superconvergent scheme for aeroacoustics. *INRIA Research Report*, *RR-5212*, 2004.
13. Dreyer M, Schmid U. Testcase 3: reorientation of a liquid surface after a step reduction of the gravity. *Experimental Results of the COMPERE TEST CASES 1*, *2 and 3*, November 2000.
14. Woelk G, Dreyer M, Rath HJ. Damped oscillations of a liquid/gas surface upon step reduction in gravity. *Journal of Spacecraft and Rockets* 1997; **34**(1).

DOI: 10.1002/fld